Available online at www.sciencedirect.com
SCIENCE DIRECT
Solid State Sciences 7 (2005) 59–66
Solid State Sciences
www.elsevier.com/locate/ssscie

The nonstoichiometric ternary cerium iron sulfide $Ce_2Fe_{1.82}S_5$

Wiebke Harms [a], Allison M. Mills [a], Tilo Söhnel [a], Clemens Laubschat [b], Friedrich E. Wagner [c], Christoph Geibel [d], Zakir Hossain [d], Michael Ruck [a,*]

[a] *Institut für Anorganische Chemie, Technische Universität Dresden, 01062 Dresden, Germany*
[b] *Institut für Festkörperphysik, Technische Universität Dresden, 01062 Dresden, Germany*
[c] *Physik-Department, Technische Universität München, 85747 Garching, Germany*
[d] *Max-Planck-Institut für Chemische Physik fester Stoffe, Nöthnitzer Straße 40, 01187 Dresden, Germany*

Received 27 February 2004; received in revised form 26 September 2004; accepted 10 October 2004

Available online 8 December 2004

Abstract

The nonstoichiometric ternary cerium iron sulfide $Ce_2Fe_{1.82(6)}S_5$ was synthesized through reaction of the elements in a LiCl/KCl flux at 1120 K, and its structure was determined by single-crystal X-ray diffraction. $Ce_2Fe_{1.82}S_5$ crystallizes in the polar orthorhombic space group $Pmn2_1$ with $a = 3.9590(2)$ Å, $b = 16.413(1)$ Å, $c = 11.2362(9)$ Å and $Z = 4$. The structure is a defect variant of the $La_2Fe_2S_5$ structure type. The parent structure contains both octahedral and tetrahedral iron sites, within one-dimensional chains of edge-sharing $[FeS_x]$-polyhedra that run along the [100] direction. In $Ce_2Fe_{1.82}S_5$, vacancies occur exclusively in the octahedral iron sites. The "tetrahedral" iron sites are split into three closely spaced partially occupied positions with coordination numbers of $[4 + 1]$. The presence of vacancies entails the partial oxidation of one of the cations to compensate the charge. The X-ray absorption near-edge structure (XANES) of the Ce $M_{IV,V}$ edge of $Ce_2Fe_{1.82}S_5$ showed no evidence of the occurrence of tetravalent cerium. The presence of Fe^{3+} was unambiguously established on the basis of hyperfine fields observed in a ^{57}Fe-Mößbauer spectrum at 4.2 K. The temperature dependence of the reciprocal magnetic susceptibility (χ^{-1}) of $Ce_2Fe_{1.82}S_5$ is nearly linear at higher temperatures. A rapid decrease in χ^{-1} below approximately 90 K suggests a ferrimagnetic transition.

Keywords: Mixed-valence; Crystal structure; XANES; Mößbauer spectroscopy; Magnetic properties; Cerium; Iron

1. Introduction

The ternary R–T–S system (R = rare-earth metal, T = transition metal) is a potential source for materials with interesting magnetic properties originating from the interplay of rare-earth and transition metal moments [1]. As a starting point for our investigation of mixed metal sulfides, we have chosen to focus on the Ce–Fe–S system. Few cerium iron sulfides have been reported to date, and prior to our work, none had been well characterized. Early studies of the pseudo-binary Ce_2S_3–FeS system revealed the existence of three compounds: "Ce_4FeS_7" [2], "Ce_2FeS_4" [3] and "$Ce_2Fe_2S_5$" [3]. We have recently determined the structure of "Ce_4FeS_7" by single-crystal X-ray diffraction [4]. The compound, which has an actual composition closer to $Ce_3Fe_2S_7$, adopts the $Ce_6Al_{3.33}S_{14}$ structure type [5]. The "Ce_2FeS_4" phase was originally characterized by powder X-ray diffraction as being monoclinic [3], but now seems likely to be of the rhombohedral $La_{32.66}Fe_{11}S_{60}$ structure type [6,7]. A single-crystal structure determination has yet to be carried out.

The "$Ce_2Fe_2S_5$" phase is the subject of this communication. The only previous mention of this compound was made in 1968 by Patrie and co-workers, who reported its orthorhombic cell parameters, calculated from powder diffraction data [3]. Since "$Ce_2Fe_2S_5$" is assumed to be isostructural to the lanthanum analogue $La_2Fe_2S_5$ [8,9], the orig-

* Corresponding author.
E-mail address: michael.ruck@chemie.tu-dresden.de (M. Ruck).

1293-2558/$ – see front matter
doi:10.1016/j.solidstatesciences.2004.10.004

inal chemical formula seems to be correct in this case. The $La_2Fe_2S_5$ structure type is rather unusual, since it contains Fe^{2+} in both octahedral and tetrahedral sites. The $[FeS_6]$-octahedra share *trans*-edges to form linear chains; the $[FeS_4]$-tetrahedra bridge pairs of octahedra within the chains by sharing edges with them. The resulting chains of $[FeS_x]$-polyhedra run along the [100] direction, with all of the $[FeS_4]$-tetrahedra on the same side. Thus, the structure is polar and one-dimensional in character, favoring anisotropic physical properties.

Our goal was to prepare $Ce_2Fe_2S_5$, in order to clarify its crystal structure and to characterize its magnetic properties. Combined magnetization and neutron diffraction studies on $La_2Fe_2S_5$ have shown that the lanthanum compound is antiferromagnetic between 88 and 17 K, and weakly ferromagnetic below 17 K [10–12]. Substitution of nonmagnetic La^{3+} $(4f^0)$ by Ce^{3+} $(4f^1)$ makes additional coupling interactions possible and should lead to more complex magnetic behavior. In our attempt to synthesize $Ce_2Fe_2S_5$, we isolated the nonstoichiometric title compound $Ce_2Fe_{1.82}S_5$ instead. Its crystal structure, which bears some similarity to those described for the two known lanthanum defect variants $La_2Fe_{1.87}S_5$ [9] and $La_2Fe_{1.76}S_5$ [13], is reported here. We also report its characterization by X-ray absorption near-edge structure (XANES) and Mößbauer spectroscopy, and by magnetic susceptibility measurements.

2. Experimental

2.1. Synthesis and chemical analysis

The nonstoichiometric compound $Ce_2Fe_{1.82}S_5$ was prepared during an attempt to synthesize the stoichiometric compound $Ce_2Fe_2S_5$. Initially, reaction of the binary sulfides Ce_2S_3 and FeS, according to the literature method, was tried [9]. However, the product obtained using this method was invariably an impure powder. Crystals of $Ce_2Fe_{1.82}S_5$ were isolated from a reaction of the elements in an alkali metal chloride flux. Starting reactants were cerium (pieces, 99.9%, TBL-Kelpin; freshly filed prior to use), iron (powder, 99.99%, ABCR), and sulfur (powder, > 99%, VEB Laborchemie; recrystallized from CS_2, then purified of carbon according to the method of von Wartenberg [14]). A 1:1 mixture of LiCl (p.a., Merck) and KCl (p.a., J.T. Baker), which was first heated under dynamic vacuum to remove any moisture, was used as a flux. The elements Ce, Fe and S, in a ratio of 2:2:5 (0.5 g in total), were combined with the LiCl/KCl flux (1 g) in a fused silica ampule (6-cm length, 0.8-cm diameter), which was then sealed under vacuum (10^{-3} Torr). The reaction mixture was heated at 1120 K for six days, then cooled to room temperature at a rate of 5 K h^{-1}. The flux was removed by washing the sample several times with water then ethanol. The resulting product contained silver-colored needles of $Ce_2Fe_{1.82}S_5$, as well as red ($Ce_{10}S_{14}O$ [15]) and gray (FeS [16]) powders. The composition of the crystals was determined by energy-dispersive X-ray (EDX) analyses on a CamScan CS44 scanning electron microscope; anal. (mol%): Ce 25(1), Fe 21.2(4), S 54(1) (average of 5 analyses). Powder X-ray diffraction analysis on a Siemens D5000 diffractometer indicated the presence of approximately 8% each of $Ce_{10}S_{14}O$ and FeS in the product, in addition to the major phase, $Ce_2Fe_{1.82}S_5$. The powder samples used in the subsequent physical characterization were prepared by grinding single crystals of $Ce_2Fe_{1.82}S_5$.

2.2. X-ray structure determination

An initial investigation of the reciprocal lattice of a single crystal of $Ce_2Fe_{1.82}S_5$ was performed using a Buerger precession camera. Diffraction images displayed strong reflections that could be indexed according to the cell of the $La_2Fe_2S_5$ structure, in space group $Cmc2_1$. However, additional weak reflections violated the systematic reflection conditions of the space group, in particular that for C-centering (hkl: $h + k = 2n$). When all reflections were considered, the observed reflection conditions ($h0l$:

Table 1
Crystallographic data and details of the structure determination for $Ce_2Fe_{1.82}S_5$

Formula	$Ce_2Fe_{1.82(6)}S_5$
Formula weight	542.19
Crystal system, space group	Orthorhombic, $Pmn2_1$ (No. 31)
Cell parameters	$a = 3.9590(2)$ Å, $b = 16.413(1)$ Å, $c = 11.2362(9)$ Å, $V = 730.12(8)$ Å^3
Formula units per cell	$Z = 4$
Calculated density	$\rho_{calc} = 4.93$ g cm^{-1}
Crystal dimensions	0.37 mm × 0.20 mm × 0.18 mm
Temperature	293 K
Measurement device	Image-plate diffractometer (STOE IPDS-II)
Radiation	Graphite-monochromated Mo-K$_\alpha$ ($\lambda = 0.71073$ Å)
Measurement limits	$4.40° \leqslant 2\theta \leqslant 54.16°$, $-5 \leqslant h \leqslant 4$, $-20 \leqslant k \leqslant 20$, $-14 \leqslant l \leqslant 14$
Scan type	$0 \leqslant \omega \leqslant 180°$, $\Delta\omega = 1°$; $\phi_1 = 0$, $\phi_2 = 45°$
Absorption correction	Numerical, on the basis of a crystal description optimized using equivalent reflections [17,18]
Absorption coefficient	μ(Mo-K$_\alpha$) = 171 cm^{-1}
Transmission factors	0.046 to 0.125
Number of reflections	5790 measured, 1833 independent
Data averaging	$R_{int} = 0.051$, $R_\sigma = 0.036$
Structure refinement	Full-matrix least-squares on F_o^2 [19]; anisotropic displacement parameters, isotropic for Fe(1a–1c) and Fe(2a–2c)
Extinction parameter	0.038(2)
Number of parameters, restraints	121, 3
Residual electron density	+2.38 to −1.75 e Å^{-3}
Figures of merit	R_1 (all 1833 F_o) = 0.039, R_1 (1665 $F_o > 4\sigma(F_o)$) = 0.038, wR_2 (all 1833 F_o) = 0.104
Goodness of fit	$S = 1.05$

Table 2
Wyckoff positions, occupancies (k), and positional and equivalent isotropic displacement parameters for $Ce_2Fe_{1.82}S_5$. The U_{eq} values (in pm^2) are defined as one-third of the trace of the orthogonalized U_{ij} tensor. All atoms lie on the mirror plane at $x = 0$

Atom	Wyckoff	k	y	Z	U_{eq}/U_{iso}
Ce(1)	2*a*	1	0.62562(4)	0.35105(6)	166(4)
Ce(2)	2*a*	1	0.62732(3)	0.73217(6)	144(3)
Ce(3)	2*a*	1	0.87055(3)	0.22489(6)	149(3)
Ce(4)	2*a*	1	0.87504(4)	0.83892(6)	174(4)
Fe(1a)	2*a*	0.387(8)	0.1810(5)	0.0000(6)	159(5)
Fe(1b)	2*a*	0.575(9)	0.1634(2)	0.0122(4)	159(5)
Fe(1c)	2*a*	0.038(5)	0.224(3)	0.002(4)	159(5)
Fe(2a)	2*a*	0.358(7)	0.3071(6)	0.4981(6)	160(6)
Fe(2b)	2*a*	0.52(1)	0.3285(3)	0.5080(5)	160(6)
Fe(2c)	2*a*	0.124(5)	0.267(1)	0.511(1)	160(6)
Fe(3)	2*a*	0.913(9)	0.5498(1)	0.0576(2)	225(7)
Fe(4)	2*a*	0.734(9)	0.9521(1)	0.5473(3)	250(10)
S(1)	2*a*	1	0.4883(2)	0.1888(3)	200(7)
S(2)	2*a*	1	0.0524(2)	0.8873(3)	197(7)
S(3)	2*a*	1	0.1053(2)	0.5364(3)	197(6)
S(4)	2*a*	1	0.2441(2)	0.8240(3)	159(5)
S(5)	2*a*	1	0.2547(2)	0.3180(3)	179(6)
S(6)	2*a*	1	0.3998(2)	0.0451(3)	173(6)
S(7)	2*a*	1	0.4455(2)	0.3996(3)	188(7)
S(8)	2*a*	1	0.4520(2)	0.7023(3)	184(7)
S(9)	2*a*	1	0.7054(2)	0.0968(3)	194(6)
S(10)	2*a*	1	0.7900(2)	0.5899(3)	203(6)

Table 3
U_{ij} coefficients (in pm^2) of the tensors of the anisotropic displacement parameters of the form $\exp\{-2\pi^2[U_{11}h^2a^{*2} + U_{22}k^2b^{*2} + U_{33}l^2c^{*2} + 2U_{12}hka^*b^* + 2U_{13}hla^*c^* + 2U_{23}klb^*c^*]\}$. The U_{12} and U_{13} coefficients for all atoms are required by symmetry to be zero

Atom	U_{11}	U_{22}	U_{33}	U_{23}
Ce(1)	99(4)	176(4)	224(9)	26(2)
Ce(2)	106(4)	152(3)	175(7)	−22(2)
Ce(3)	105(4)	157(3)	184(7)	20(3)
Ce(4)	101(4)	161(4)	260(10)	−19(2)
Fe(3)	220(10)	181(9)	270(10)	16(8)
Fe(4)	220(10)	210(10)	310(20)	−50(10)
S(1)	160(10)	190(10)	240(20)	−30(10)
S(2)	230(10)	120(10)	240(20)	50(10)
S(3)	130(10)	320(10)	150(10)	−50(10)
S(4)	110(10)	150(10)	220(10)	−40(10)
S(5)	120(10)	130(10)	280(10)	30(10)
S(6)	110(10)	270(10)	140(10)	40(10)
S(7)	180(10)	150(10)	230(20)	−50(10)
S(8)	120(10)	190(10)	240(20)	0(10)
S(9)	130(10)	240(10)	210(20)	−40(10)
S(10)	130(10)	280(10)	210(20)	30(10)

$h + l = 2n$; $00l$: $l = 2n$) were uniquely consistent with the polar orthorhombic space group $Pmn2_1$.

Intensity data for the same single crystal were collected at 293 K using graphite-monochromated Mo-K_α radiation, on a STOE IPDS-II diffractometer. Crystal data and further details of the data collection are given in Table 1. A numerical absorption correction was applied with the program X-RED [17] based on a crystal description optimized using equivalent reflections with X-SHAPE [18]. The structure was solved by direct methods using SHELXS97, and refined on F^2 using SHELXL97 [19]. After the cerium, sulfur, and four unsplit iron sites were found through repeated refinements and difference Fourier syntheses, additional residual electron density remained near the two "tetrahedral" iron sites. Closer investigation of electron density maps generated with the program ANAREF [20] clearly showed that sites Fe(1) and Fe(2) were elongated along the [010] direction. To model this positional disorder, each iron atom was split into three closely spaced positions, Fe(1a–1c) and Fe(2a–2c). The occupancies of each set of positions were constrained to sum to 1. The three split positions of each set were refined with the same isotropic displacement parameter. All other atoms were refined with anisotropic displacement parameters. Since the displacement ellipsoids of Fe(3) and Fe(4) were initially unusually large, the occupancies of the octahedral iron sites were refined freely. The resulting formula is $Ce_2Fe_{1.82(6)}S_5$, consistent with the EDX analyses. The crystal was an inversion twin, the relative fractional contributions of the twin components being 0.38(3):0.62. The atomic positions of $Ce_2Fe_{1.82}S_5$ were standardized with the program STRUCTURE TIDY [21]. Final values of the positional and displacement parameters are given in Tables 2 and 3. Selected interatomic distances and angles are listed in Tables 4 and 5. Further data, in the form of a CIF, have been deposited with the Fachinformationszentrum Karlsruhe, 76344 Eggenstein-Leopoldshafen, Germany (e-mail address: crysdata@fiz-karlsruhe.de), as supplementary material No. CSD 413747, and can be obtained by contacting the FIZ (quoting the article details and the corresponding CSD number). Graphics were prepared using the program DIAMOND [22].

Table 4
Selected interatomic distances (in pm) for $Ce_2Fe_{1.82}S_5$

Ce(1)–S(8^{i}, 8^{ii})	288.7(2)	Ce(4)–S(1^{iii}, 1^{iv})	288.9(2)
S(4^{i}, 4^{ii})	293.0(2)	S(5^{iii}, 5^{iv})	291.7(2)
S(6^{iii}, 6^{iv})	297.4(2)	S(2^{v})	296.1(3)
S(7)	300.7(3)	S(3^{iii}, 3^{iv})	299.1(2)
S(9)	314.2(3)	S(10)	312.7(3)
Ce(2)–S(8)	289.8(3)	Ce(3)–S(3^{i}, 3^{ii})	292.6(2)
S(6^{iii}, 6^{iv})	292.2(2)	S(1^{v})	294.6(3)
S(5^{iii}, 5^{iv})	293.3(2)	S(4^{i}, 4^{ii})	294.9(2)
S(7^{iii}, 7^{iv})	298.1(2)	S(2^{i}, 2^{ii})	297.5(2)
S(10)	311.3(3)	S(9)	307.0(3)
Fe(1a)–S(4^{vi})	223.2(7)	Fe(2a)–S(5)	220.0(7)
S(10^{i}, 10^{ii})	227.2(3)	S(9^{iii}, 9^{iv})	227.8(4)
S(2^{vi})	246.2(8)	S(7)	253(1)
S(6)	304.1(8)	S(8)	330.3(8)
Fe(1b)–S(10^{i}, 10^{ii})	229.5(3)	Fe(2b)–S(7)	227.3(6)
S(2^{vi})	230.0(5)	S(9^{iii}, 9^{iv})	228.6(3)
S(4^{vi})	249.5(5)	S(5)	245.5(6)
S(1)	274.0(5)	S(8)	297.8(6)
Fe(1c)–S(4^{vi})	202(5)	Fe(2c)–S(5)	218(1)
S(10^{i}, 10^{ii})	223(2)	S(9^{iii}, 9^{iv})	224.8(6)
S(6)	292(5)	S(3)	267(2)
S(2^{vi})	310(5)	S(7)	319(2)
Fe(3)–S(6)	246.6(3)	Fe(4)–S(3^{v})	251.7(4)
S(8^{i}, 8^{ii})	256.1(3)	S(1^{iii}, 1^{iv})	253.9(3)
S(9)	259.0(4)	S(2^{i}, 2^{ii})	267.5(3)
S(7^{i}, 7^{ii})	266.0(3)	S(10)	270.2(4)
Ce···Ce	> 396	Fe···Fe	> 277
Fe	> 351	S···S	> 323

Symmetry operations: ^{i} $-1/2-x, 1-y, -1/2+z$; ^{ii} $1/2-x, 1-y, -1/2+z$; ^{iii} $-1/2-x, 1-y, 1/2+z$; ^{iv} $1/2-x, 1-y, 1/2+z$; ^{v} $x, 1+y, z$; ^{vi} $x, y, -1+z$.

Table 5
Selected bond angles (in deg) for $Ce_2Fe_{1.82}S_5$

S(2)–Fe(1a)–S(4)	86.7(2)	S(5)–Fe(2a)–S(7)	87.1(3)
S(4)–Fe(1a)–S(10)	107.3(5)	S(7)–Fe(2a)–S(9)	107.1(3)
S(2)–Fe(1a)–S(10)	114.1(2)	S(5)–Fe(2a)–S(9)	114.4(2)
S(10)–Fe(1a)–S(10)	121.2(3)	S(9)–Fe(2a)–S(9)	120.7(3)
S(7)–Fe(3)–S(8)	81.29(7)	S(1)–Fe(4)–S(2)	81.02(8)
S(8)–Fe(3)–S(9)	84.46(9)	S(1)–Fe(4)–S(10)	83.5(1)
S(6)–Fe(3)–S(7)	89.46(9)	S(2)–Fe(4)–S(3)	89.7(1)
S(6)–Fe(3)–S(8)	91.42(9)	S(1)–Fe(4)–S(3)	91.9(1)
S(7)–Fe(3)–S(9)	94.9(1)	S(2)–Fe(4)–S(10)	95.3(1)
S(7)–Fe(3)–S(7)	96.2(1)	S(2)–Fe(4)–S(2)	95.5(1)
S(8)–Fe(3)–S(8)	101.2(1)	S(1)–Fe(4)–S(1)	102.4(2)
S(6)–Fe(3)–S(9)	173.5(2)	S(3)–Fe(4)–S(10)	172.6(2)
S(7)–Fe(3)–S(8)	177.3(1)	S(1)–Fe(4)–S(2)	176.1(1)

2.3. X-ray absorption near edge structure (XANES) spectroscopy

X-ray absorption near-edge structure (XANES) measurements were performed at the Russian–German Beamline (RGBL) of BESSY II (Berlin). The Ce $M_{IV,V}$ and Fe $L_{II,III}$ edges were recorded for a single crystal of $Ce_2Fe_{1.82}S_5$, and for powders of several reference compounds: α-Ce_2S_3 (slightly contaminated with $Ce_{10}S_{14}O$), CeS_2, FeS, $KFeS_2$ (slightly contaminated with FeS_2 and Fe_7S_8) and α-Fe_2O_3. The single crystal was pressed onto a piece of indium foil, in order to fix it to the sample holder. The powders were rubbed onto a scratched copper plate. Experiments were carried out under ultra-high vacuum, in total electron yield mode. Samples were heated inside the vacuum chamber at 420 K for 20 h before their spectra were recorded at room temperature. Photon energies were calibrated based on the peak positions of the F 1*s* absorption spectrum of K_2TiF_6 and the 1*s* spectrum of neon.

2.4. Mößbauer spectroscopy

^{57}Fe-Mößbauer spectra of a powder sample of $Ce_2Fe_{1.82}S_5$ (ca. 20 mg) were recorded at 298 and 4.2 K on a noncommercial instrument at the Physics Department of the Technische Universität München. Transmission spectra were measured with a ^{57}Co source in a rhodium matrix, using α-iron as a standard. For the low temperature measurement, both the source and the absorber were cooled in a helium bath cryostat.

2.5. Magnetic measurements

Magnetic susceptibility measurements were made on powder samples of $Ce_2Fe_{1.82}S_5$ (ca. 20 mg), using a Quantum Design MPMS XL-7 SQUID magnetometer. The sample magnetization was measured from 2 to 350 K at a field of 1 T. All susceptibility values were corrected for the diamagnetic contribution of the sample.

3. Results and discussion

3.1. Description and discussion of the crystal structure

The $Ce_2Fe_{1.82}S_5$ structure, shown in Fig. 1, is a defect variant of the $La_2Fe_2S_5$ structure type ($Cmc2_1$) [8,9]. In the parent structure, there are two fully occupied iron sites, one octahedral and one tetrahedral. The [FeS_6]-octahedra share *trans*-edges to form linear $^{1}_{\infty}[Fe_{oct}S_2S_{4/2}]$-chains that run along [100]. The [FeS_4]-tetrahedra bridge pairs of octahedra on the same side of the chain, by each sharing two edges with two octahedra, and two vertices with each other. Four identical, isolated $^{1}_{\infty}[(Fe_{oct}SS_{2/2}S_{3/3})(Fe_{tet}SS_{3/3})]$-chains occur in the unit cell. In $Ce_2Fe_{1.82}S_5$, partial ordering of defects in the iron sites leads to a loss of the *C*-centering, with retention of the crystal class ($mm2$) and conventional unit cell of the parent structure. Therefore, $Ce_2Fe_{1.82}S_5$ crystallizes in space group $Pmn2_1$, a maximal *klassengleiche* subgroup of index 2 of $Cmc2_1$. The number of independent atomic positions is doubled, such that there are four independent iron sites, two octahedral and two "tetrahedral". Vacancies occur exclusively in the octahedral sites, Fe(3) and Fe(4). To

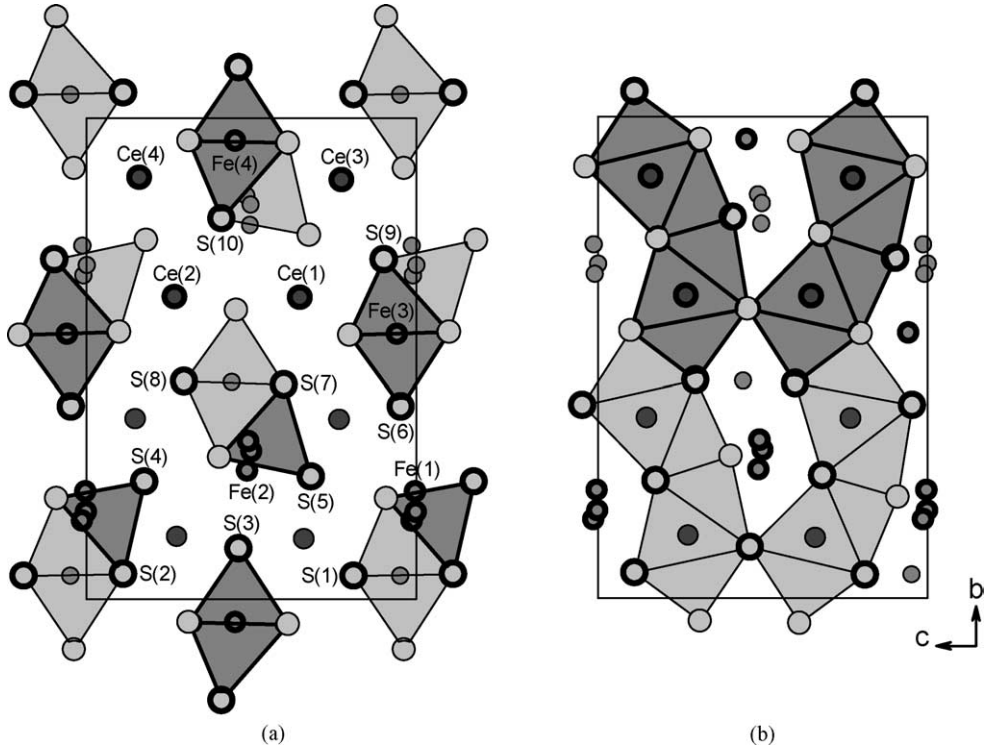

Fig. 1. Views down the [100] direction of the crystal structure of $Ce_2Fe_{1.82}S_5$ highlighting (a) the iron-centered [FeS_x]-polyhedra, or (b) the cerium-centered [CeS_8]-polyhedra. The unit cell and atomic labels are indicated. All atoms reside on mirror planes at $x = 0$ or $1/2$. Atoms with thick rims are located at $x = 0$. Polyhedra centered by atoms at $x = 0$ are darker gray with thick outlines.

compensate for the defects, the neighboring, originally tetrahedrally coordinated, iron atoms shift in order to increase their coordination numbers. Each of the two "tetrahedral" sites is split into three closely spaced partially occupied positions, Fe(1a–1c) and Fe(2a–2c). Two independent chains of [FeS_x]-polyhedra (composed of Fe(1a–1c)/Fe(4) and Fe(2a–2c)/Fe(3), respectively), which differ mainly in the occupancies of the iron sites (Table 2), run through the unit cell. A view of the $Ce_2Fe_{1.82}S_5$ structure highlighting the iron-centered polyhedra is presented in Fig. 1(a).

Although they are occupied in quite different proportions, both of the octahedrally coordinated iron sites have similar coordination geometries (Fig. 2(a)). The [Fe(3)S(6)S(7)$_2$-S(8)$_2$S(9)]- and [Fe(4)S(1)$_2$S(2)$_2$S(3)S(10)]-octahedra are significantly distorted, as indicated by the *cis*- and *trans*-angles, which range from 81.0 to 102.4° and from 172.6 to 177.3°, respectively (Table 5). The Fe–S bond lengths of 246.6–270.2 pm (Table 4) are comparable to those observed in the [FeS_6]-octahedra found in the stoichiometric lanthanum compound $La_2Fe_2S_5$ (245–267 pm) [9] or the binary iron sulfide FeS (236.0–271.7 pm) [16].

Three types of split positions originate from each "tetrahedral" iron site (Fig. 2(a)). The occupancies of each set of split positions exhibit the same trend, the "b" positions having the highest occupancies, and the "c" positions the lowest. The central "a" positions resemble the tetrahedral site of $La_2Fe_2S_5$ most closely [9]. As in the parent structure, the [Fe(1a)S(2)S(4)S(10)$_2$]- and [Fe(2a)S(5)S(7)S(9)$_2$]-tetrahedra are highly distorted, with S–Fe–S angles of 86.7–121.2° that deviate considerably from the ideal value of 109.5° (Ta-

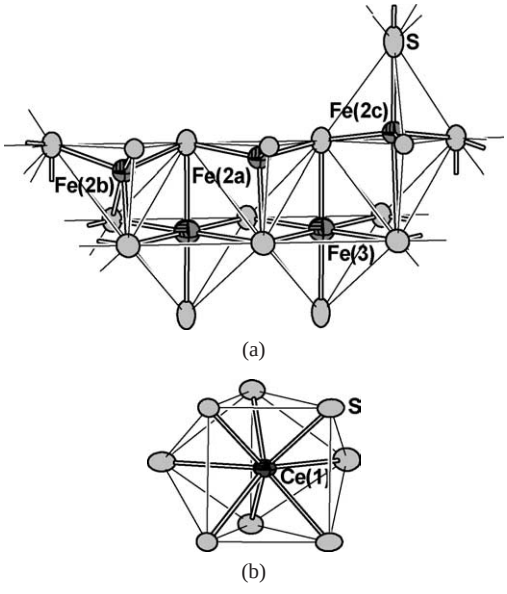

Fig. 2. Metal atom coordination environments in $Ce_2Fe_{1.82}S_5$. (a) Section of one of the two independent chains of edge-sharing [FeS_x]-polyhedra, showing the octahedral coordination environment of Fe(3) and the distorted [4 + 1] coordination environments of Fe(2a–2c). The partially occupied Fe(2a–2c) positions are presented in one possible local ordering pattern. (b) Bicapped trigonal prismatic coordination around Ce(1), one of the four independent cerium atoms. Displacement ellipsoids are drawn at the 90% probability level.

Table 6
Structural data for $R_2Fe_{2-\delta}S_5$ compounds

	δ	Space group	a (Å)	b (Å)	c (Å)	Z	Ref.
$La_2Fe_2S_5$	0	$Cmc2_1$	3.997(2)	16.485(5)	11.394(4)	4	[9]
$La_2Fe_{1.87}S_5$	0.13	$Cmc2_1$	3.9996(5)	49.508(3)	11.308(3)	12	[9]
$Ce_2Fe_{1.82}S_5$	0.18	$Pmn2_1$	3.9590(2)	16.413(1)	11.2362(9)	4	
$La_2Fe_{1.76}S_5$	0.24	$Pmc2_1$	4.001(1)	32.936(7)	11.291(3)	8	[13]

ble 5). The Fe–S distances of 220–253 pm within the distorted tetrahedra (Table 4) span a larger range than those in $La_2Fe_2S_5$ (230–237 pm). The next shortest Fe–S distances involve S atoms from [FeS_6]-octahedra within the [FeS_x]-chain: the Fe(2a)–S(8) distance of 330.3(8) pm is slightly longer than the analogous distance in $La_2Fe_2S_5$ (325(2) pm), while the Fe(1a)–S(6) distance of 304.1(8) pm is considerably shorter. The tendency towards [4 + 1] coordination is more pronounced for the "b" and "c" positions, which are shifted towards nearby sulfur atoms, within the same [FeS_x]-chain (S(1) or S(8)) or a neighboring chain (S(2) or S(7)), respectively. The resulting coordination polyhedra have geometries approaching trigonal bipyramidal.

The chains of [FeS_x]-polyhedra are connected by the cerium atoms, which occupy four independent sites. All are eight-coordinate, with a similar bicapped trigonal prismatic coordination environment of sulfur atoms (Fig. 2(b)). As shown in Fig. 1(b), the cerium-centered prisms share trigonal faces to form columns along [100]. The columns are linked into a three-dimensional network through further edge- and face-sharing of the [CeS_8]-bicapped trigonal prisms. The four cerium sites can be grouped into two sets: Ce(1) and Ce(4), which each share two edges and one face with [FeS_6]-octahedra, in addition to four vertices with [FeS_4]-"tetrahedra"; and Ce(2) and Ce(3), which each share three edges and one vertex with [FeS_6]-octahedra, in addition to two edges and one vertex with [FeS_4]-"tetrahedra". The coordination environment of the cerium atoms is little affected by the defects in the [FeS_x]-chains, and resembles that observed in $La_2Fe_2S_5$ quite closely [9]. Capped rare-earth-centered trigonal prisms are commonly observed in ternary rare-earth sulfides. The Ce–S distances of 288.7–314.2 pm found in $Ce_2Fe_{1.82}S_5$ (Table 4) are similar to those found in the [CeS_7]-monocapped trigonal prisms of $Ce_3Fe_2S_7$ (284.3–303.7 pm) [4], or the [CeS_8]-bicapped trigonal prisms of Ce_2SiS_5 (279.2–308.0 pm) [23].

The $Ce_2Fe_{1.82}S_5$ structure is the newest member of a family of superstructures derived from $La_2Fe_2S_5$ that also includes the nonstoichiometric $La_2Fe_{1.87}S_5$ [9] and $La_2Fe_{1.76}S_5$ [13] structures. Structural data for the $R_2Fe_{2-\delta}S_5$ compounds are listed in Table 6. All of the superstructures result from a partial ordering of defects in the iron sites and an associated shifting of neighboring sites. The member with the smallest number of vacancies, $La_2Fe_{1.87}S_5$, retains the $Cmc2_1$ space group type of the parent structure, but has a unit cell that is three times as big ($Z = 12$), as a result of a tripling of the b cell parameter. There are three independent chains of [FeS_x]-polyhedra in the asymmetric unit: one with fully occupied iron sites, one with defects in the tetrahedral sites and one with defects in the octahedral sites. The second lanthanum defect structure, $La_2Fe_{1.76}S_5$, crystallizes in the space group $Pmc2_1$, a *klassengleiche* subgroup of $Cmc2_1$, with a unit cell that is twice as large as that of $La_2Fe_2S_5$ ($Z = 8$), owing to a doubled b cell parameter. The asymmetric unit contains four independent [FeS_x]-chains. The iron sites are fully occupied in only one of the chains. Of the remaining three, one has defects in the tetrahedral iron sites, and the other two have defects in the octahedral sites. In both the $La_2Fe_{1.87}S_5$ and the $La_2Fe_{1.76}S_5$ structures, the [FeS_x]-chains with no vacancies or with vacancies in the "tetrahedral" sites differ little from those in stoichiometric $La_2Fe_2S_5$. In the [FeS_x]-chains with vacancies in the octahedral sites, on the other hand, the "tetrahedral" site is shifted towards a sulfur atom from an [FeS_6]-octahedron within the same chain, resulting in a [4 + 1] coordination similar to that observed for the "b" positions in $Ce_2Fe_{1.82}S_5$.

The presence of cation vacancies in $La_2Fe_{1.87}S_5$ and $La_2Fe_{1.76}S_5$ entails the partial oxidation of Fe^{2+} to Fe^{3+} for the preservation of charge balance [9,13]. Thus, the formulae of the lanthanum compounds can be expressed as $(La^{3+})_2(Fe^{3+})_{2\delta}(Fe^{2+})_{2-3\delta}\square_\delta S_5$. In the case of $Ce_2Fe_{1.82}S_5$, the situation is less clear since, unlike lanthanum, cerium can exist in both the +4 and +3 oxidation states.

3.2. X-ray absorption near-edge structure (XANES) spectroscopy

In order to clarify the assignment of oxidation states in $Ce_2Fe_{1.82}S_5$, X-ray absorption near-edge structure (XANES) spectra were collected at the Ce $M_{IV,V}$ and Fe $L_{II,III}$ absorption edges of $Ce_2Fe_{1.82}S_5$ and several reference compounds.

The Ce $M_{IV,V}$ absorption edges of $Ce_2Fe_{1.82}S_5$ and the two Ce^{3+} reference compounds, α-Ce_2S_3, and CeS_2, presented in Fig. 3(a), resemble each other closely. All display the characteristic multiplet structure of the localized $3d^94f^2$ configuration [24]. The energy positions of the absorption edges are also quite similar. The spectra of $Ce_2Fe_{1.82}S_5$ and α-Ce_2S_3, in particular, are nearly identical. The absence of any new features, arising from an overlapping Ce^{4+} spectrum, in the spectrum of $Ce_2Fe_{1.82}S_5$ suggests a pure Ce^{3+} oxidation state in this compound.

As shown in Fig. 3(b), the Fe $L_{II,III}$ absorption spectra of $Ce_2Fe_{1.82}S_5$, the Fe^{2+} reference compound FeS, and the Fe^{3+} reference compounds $KFeS_2$ and α-Fe_2O_3 differ more noticeably from one another. The absorption edges of the two Fe^{3+} reference compounds are shifted to higher energies

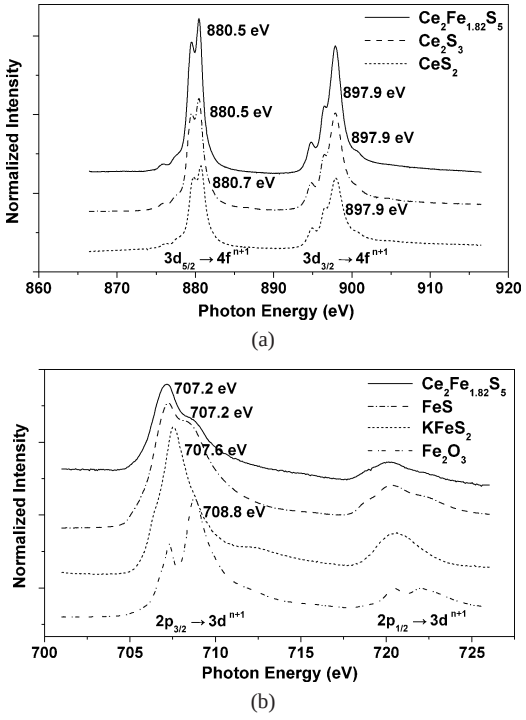

Fig. 3. XANES spectra of $Ce_2Fe_{1.82}S_5$. (a) Ce $M_{IV,V}$ absorption edges of $Ce_2Fe_{1.82}S_5$ and the reference compounds α-Ce_2S_3 and CeS_2. (b) Fe $L_{II,III}$ absorption edges of $Ce_2Fe_{1.82}S_5$ and the reference compounds FeS, $KFeS_2$ and α-Fe_2O_3.

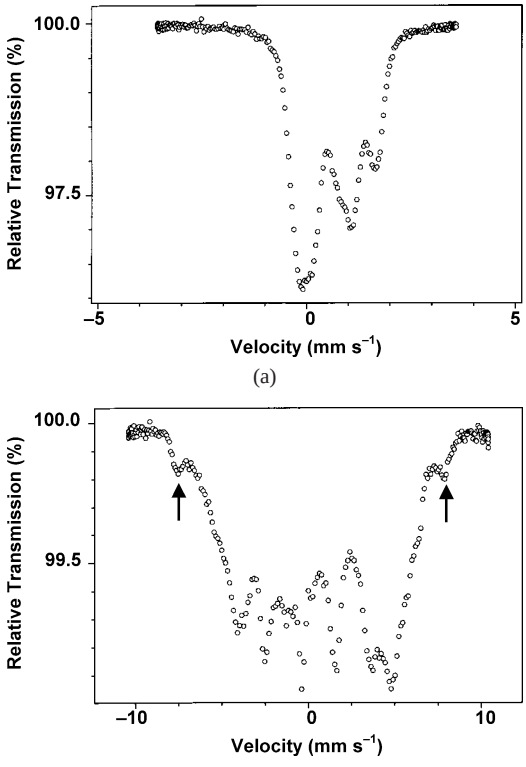

Fig. 4. Mößbauer spectra of $Ce_2Fe_{1.82}S_5$ at (a) 295 K and (b) 4.2 K. Magnetic ordering is observed in the 4.2 K spectrum. The quadrupole sextet with the largest hyperfine splitting (outer lines indicated by arrows) confirms the presence of Fe^{3+}.

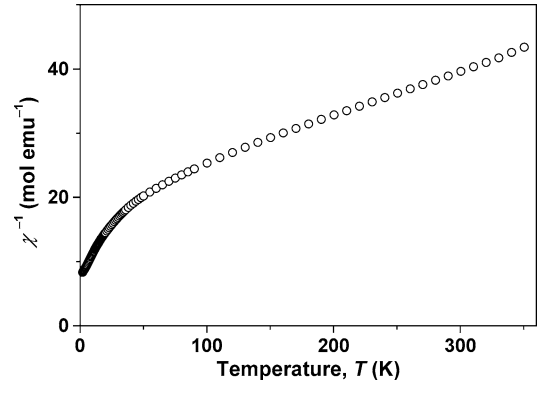

Fig. 5. Temperature dependence of the reciprocal susceptibility (χ^{-1}) of $Ce_2Fe_{1.82}S_5$ at a field of 1 T.

relative to those of $Ce_2Fe_{1.82}S_5$ and FeS. The forms of the absorption edges of $KFeS_2$ and α-Fe_2O_3 are quite different from one another, as a result of the different iron coordination environments of $KFeS_2$ ($[Fe^{3+}S_4]$-tetrahedra [25]) and α-Fe_2O_3 ($[Fe^{3+}O_6]$-octahedra [26]). The forms and energies of the absorption edges of $Ce_2Fe_{1.82}S_5$ and FeS, on the other hand, are very similar. It seems clear that iron occurs mainly as Fe^{2+} in $Ce_2Fe_{1.82}S_5$. In both spectra, the main peak of the L_{III} edge has a shoulder on the high-energy side; however, the relative intensity of this shoulder is lower for $Ce_2Fe_{1.82}S_5$. This small difference could perhaps be attributed to differences in the local iron environments, since FeS contains only $[FeS_6]$-octahedra [16], while $Ce_2Fe_{1.82}S_5$ contains $[FeS_4]$-tetrahedra as well. Alternatively, the difference could be a consequence of a small Fe^{3+} content in $Ce_2Fe_{1.82}S_5$.

3.3. Mößbauer spectroscopy

The valence state of the iron atoms in $Ce_2Fe_{1.82}S_5$ was further investigated using Mößbauer spectroscopy. The spectra collected for $Ce_2Fe_{1.82}S_5$ at 298 and 4.2 K are presented in Fig. 4. Because of the large number of independent iron sites, the spectra are quite complicated. Although a detailed interpretation is beyond the scope of this paper, a few important features will be noted.

The 298 K spectrum consists of overlapping quadrupole doublets. The absence of further splitting of the $I_g = 1/2$ and $I_e = 3/2$ states implies that the compound is not magnetically ordered at room temperature. In the 4.2 K Mößbauer spectrum of $Ce_2Fe_{1.82}S_5$, however, hyperfine splitting signaling the presence of magnetic ordering is clearly visible. Of the multiple overlapping quadrupole sextets, the one with the largest hyperfine splitting (outer lines indicated with arrows in Fig. 4(b)) unambiguously establishes the presence of Fe^{3+}, which has a significantly stronger hyperfine field versus that of Fe^{2+} [27,28].

3.4. Magnetic properties

To determine the underlying nature of the magnetic ordering observed in the low-temperature Mößbauer spectrum of $Ce_2Fe_{1.82}S_5$, magnetic susceptibility measurements were carried out. The temperature dependence of the reciprocal magnetic susceptibility (χ^{-1}) of $Ce_2Fe_{1.82}S_5$ at a field of 1 T is shown in Fig. 5. At temperatures above approximately 90 K, the $\chi^{-1}(T)$ curve is nearly linear, but at lower temperatures, the $\chi^{-1}(T)$ curve departs from linearity, as χ^{-1} decreases rapidly. This behavior suggests a transition to a ferrimagnetically ordered state.

Further clarification of the magnetic ordering at low temperatures will require more detailed study. Our intention is to first prepare and investigate stoichiometric $Ce_2Fe_2S_5$, since analysis of the magnetic behavior should be more straightforward for the simpler valence-precise compound. However, our preliminary measurements reveal that the magnetic properties of $Ce_2Fe_{1.82}S_5$ clearly depart from those observed for $La_2Fe_2S_5$ [10–12], confirming our expectation that substitution of nonmagnetic La^{3+} ($4f^0$) by Ce^{3+} ($4f^1$) would influence the magnetic behavior of the compound.

Acknowledgements

We gratefully acknowledge the experimental help of Ms. J. Krug, and the financial support of the Deutsche Forschungsgemeinschaft (DFG) within the SFB 463.

References

[1] K. Mitchell, J.A. Ibers, Chem. Rev. 102 (2002) 1929.
[2] G. Collin, F. Rouyer, J. Loriers, C. R. Acad. Sci., Ser. C 266 (1968) 689.
[3] M. Patrie, H.-D. Nguyen, J. Flahaut, C. R. Acad. Sci., Ser. C 266 (1968) 1575.
[4] A.M. Mills, M. Ruck, Acta Crystallogr. C 60 (2004) i71.
[5] D. de Saint-Giniez, P. Laruelle, J. Flahaut, C. R. Acad. Sci., Ser. C 267 (1968) 1029.
[6] G. Collin, P. Laruelle, Acta Crystallogr. B 30 (1974) 1134.
[7] K. Cenzual, L.M. Gelato, M. Penzo, E. Parthé, Z. Kristallogr. 193 (1990) 217.
[8] G. Collin, P. Laruelle, Bull. Soc. Fr. Miner. Cristallogr. 94 (1971) 113.
[9] F. Besrest, G. Collin, J. Solid State Chem. 21 (1977) 161.
[10] R. Plumier, M. Sougi, M. Lecomte, J. Appl. Phys. 52 (1981) 2320.
[11] R. Plumier, M. Sougi, G. Collin, Solid State Commun. 14 (1974) 971.
[12] G. Collin, É. Barthélémy, O. Gorochov, C. R. Acad. Sci., Ser. C 277 (1973) 775.
[13] F. Besrest, G. Collin, J. Solid State Chem. 24 (1978) 301.
[14] H. von Wartenberg, Z. Anorg. Allg. Chem. 286 (1956) 243.
[15] T. Schleid, P. Lauxmann, Z. Anorg. Allg. Chem. 625 (1999) 1053.
[16] H.E. King Jr., C.T. Prewitt, Acta Crystallogr. B 38 (1982) 1877.
[17] X-RED 1.22, Program for data reduction, STOE & Cie, Darmstadt, Germany, 2001.
[18] X-SHAPE 1.06, Program for crystal optimization for numerical absorption correction, STOE & Cie, Darmstadt, Germany, 1999.
[19] G.M. Sheldrick, SHELX97, Programs for crystal structure determination, Universität Göttingen, Germany, 1997.
[20] K.-G. Adams, ANAREF, A general and substantially extended version of SYMREF, Universität Karlsruhe, Germany.
[21] L.M. Gelato, E. Parthé, J. Appl. Crystallogr. 20 (1987) 139.
[22] K. Brandenburg, DIAMOND, Visual crystal structure information system, Crystal Impact, Bonn, Germany, 1999.
[23] G. Gauthier, S. Jobic, M. Evain, H.-J. Koo, M.-H. Whangbo, C. Fouassier, R. Brec, Chem. Mater. 15 (2003) 828.
[24] B.T. Thole, G. van der Laan, J.C. Fuggle, G.A. Sawatzky, R.C. Karnatak, J.-M. Esteva, Phys. Rev. B 32 (1985) 5107.
[25] W. Bronger, Z. Anorg. Allg. Chem. 359 (1968) 225.
[26] L. Pauling, S.B. Hendricks, J. Amer. Chem. Soc. 47 (1925) 781.
[27] P. Gütlich, R. Link, A. Trautwein, Mössbauer Spectroscopy and Transition Metal Chemistry, Springer-Verlag, Berlin, 1978.
[28] D.C. Price, I. Maartense, A.H. Morrish, Phys. Rev. B 9 (1974) 281.